

# Methods for Secondary and Tertiary Structure Prediction of Microproteins

Julio C. Facelli <sup>1,2</sup>

<sup>1</sup> Department of Biomedical Informatics and <sup>2</sup> Utah Clinical and Translational Science Institute,  
The University of Utah, Salt Lake City, Utah

## Abstract

Microproteins are a newly recognized and rapidly growing class of small proteins, typically encoded by fewer than 100–150 codons and translated from small open reading frames (smORFs). Although research has shown that smORFs and their corresponding microproteins constitute a significant portion of the genome and proteome, there is still limited information available in the literature regarding the structural characteristics of microproteins. In this paper, we discuss the methods available for predicting their secondary and tertiary structures and provide examples of calculations done with three archetypical methods (AlphaFold, I-TASSER and ROSETTA). We present results predicting the structures of 44 microproteins. For this set of microproteins the methods considered here show a reasonable agreement among them and with the very few cases in which experimental structures are available. None-the-less, the agreement with experimental structures is not as good as for larger proteins, indicating that it is necessary to obtain a much larger set of experimental microproteins structures to better evaluate and eventually calibrate prediction methods.

**Keywords:** Protein Structure; Protein Structure Prediction, Microproteins

**Julio C. Facelli:** julio.facelli@utah.edu

## Introduction

Microproteins are a recently identified class of proteins encoded by small open reading frames (smORFs) containing approximately 100–150 codons. Studies have shown that smORFs and their corresponding microproteins represent a substantial portion of the genome and proteome. However, there is limited information in the literature regarding the structural characteristics of these proteins. Gaining insight into their structural and functional properties is essential for understanding their biological roles. Detecting polypeptides produced by smORFs confirms their protein-coding potential by demonstrating stable protein expression and helps distinguish bona fide microproteins from small peptide fragments generated through post-translational cleavage of larger proteins (1, 2). Although the structural study of microproteins is still in its early stages, emerging research suggests that elucidating their structures and mechanisms of action could significantly enhance our understanding of their roles in various biological processes, including disease-related pathways (1-3). The state of the art in microprotein identification, function and structure has been recently reviewed (4).

Previous studies have primarily characterized microproteins by investigating their functional properties using various experimental and functional approaches (1-3). However, these methods have limitations when it comes to analyzing the structural features of microproteins, particularly in three-dimensional detail. There are very few experimental structures that have been determined for microproteins, for instance a search for the keyword “microprotein” performed Dec. 10 of 2024 in the PDB (5), show only 11 structures associated with this nomenclature and from these ones only three correspond to the isolated microproteins, therefore computational approaches are a key tool for the understanding of microprotein structures.

In this work, we explore the available methods for protein structure determination, focusing on computational structure prediction and analytical approaches. Our goal is to further elucidate

the properties of microproteins as a group and to investigate whether they possess distinct structural features that differentiate them from larger proteins

Recent advances in the accuracy of protein structure prediction methods, combined with the significant experimental challenges of determining microprotein structures (6-9) highlight the importance of computational approaches in this area. Protein structure prediction techniques employ various strategies, including comparative modeling (10), de novo or ab initio methods (11), and machine learning-based approaches (12, 13) to infer three-dimensional structures from amino acid sequences.

Comparative modeling, also known as template-based modeling, relies on homologous sequences and their known crystal structures to build structural models. Ab initio prediction, on the other hand, uses empirical force fields or knowledge-based energy functions to estimate the most probable structures based on energy minimization and statistical conformational probabilities. More recently, machine learning particularly deep learning, has had a transformative impact on the field. Notably, AlphaFold (12, 13) has emerged as the leading method for protein structure prediction, as demonstrated in recent Critical Assessment of protein Structure Prediction (CASP) experiments (6, 8, 9, 14, 15).

## Methods

Here we used three archetypical methods, I-TASSER (16-19) as exemplar for comparative modeling, ROSETTA (20-23) as exemplar for de novo/ab initio, and AlphaFold (12, 13) as exemplar for machine learning, to compare their results for a set of 44 amino acid sequences that have been reported as genuine microproteins in the previous literature (2, 24). This paper reports

on the results of using these computational modeling methods to characterize the structural properties of 44 unique microproteins. The microproteins were selected following these criteria:

- The sequences contain less than 100 amino acids in length
- Proteins are single domain i.e. not a part of a larger sequence
- Proteins have been reported as microproteins in the published literature (1-3)

The FASTA files for the 44 microproteins sequences considered here were manually downloaded from UniProt (25). When possible, we compare the predicted structures with their experimental ones (or for similar amino acid sequences) that were found in the PDB as October 16<sup>th</sup> 2024. The microproteins studies here are listed in Table 1.

**Table 1.** Microproteins Considered in this Study. Adapted from Reference (24).Original data was manually downloaded from Uniprot (25).

Full Name	UniProt ID	Length	Sequence
60S ribosomal protein L41	P62945	25	MRAKWRKKRMRRRKRR RKMRQRSK
Apelin receptor early endogenous ligand	P0DMC3	54	MRFQQFLFAFFIFIMSLLLIS GQRPVNLTMRRLRKHNC LQRRCMPLHSRVPFP
ATP synthase subunit epsilon, mitochondrial	P56381	51	MVAYWRQAGLSYIRYSQI CAKAVRDALKTEFKANAE KTSGSNVKIVVKKE
Beta-theraphotoxin-Cm1a	P84507	33	DCLGWFKSCDPKNDKCCK NYTCSRDRWCKYDL
B melanoma antigen 4	Q86Y28	39	MAAGAVFLALSAQLLQAR LMKEESPVVSWWLEPEDG TAL
Small integral membrane protein 22	K7EJ46	83	MAVSTEELEATVQEVLGR LKSHQFFQSTWDTVAFIVF LTFMGTVLLLLLVAHC CCCSSPGPRRESPRKERPK GVDNLALEP
Conotoxin PIVE	P0C2C5	24	DCCGVKLEMCHPCLCDNS CKNYGK
DDIT3 upstream open reading frame	P0DPQ6	34	MLKMSGWQRQSQNQSWN LRRECSRRKCIFIHHHT
Dolichyl-diphosphooligosaccharide-protein glycosyltransferase subunit 4	P0C6T2	37	MITDVQLAIFANMLGVSLF LLVVLYHYVAVNNPKKQE
Sarcoplasmic/endoplasmic reticulum calcium ATPase regulator DWORF	P0DN84	35	MAEKAGSTFSHLLVPILLI GWIVGCIIMIYVVFS

Putative protein FAM66E	P0C841	47	MLASGAESQDRYRNTPSSR IFTPGFRPTPATTEPEPGIYM FNMEPSQP
Putative gastric cancer-related gene 224 protein	Q8WZA8	35	MIPGNPSPGADLAVSKHFF SLSWFCGLLLLESKQK
Hemotin	A0A0B4K753	88	MDCFKVFEVVFQSEINPLL LIPAVATIALTLCCCYCYHG YQWIRDRRTARIEEQQAQL PLPLSRISITPGCSMVATTK LTHSRNSVDIY
Histatin-3	P15516	51	MKFFVFALILALMLSMTG ADSHAKRHHGYKRKFHEK HHSHRGYRSNYLYDN
Humanin	Q8IVG9	24	MAPRGFSCLLLTSEIDLGV KRRA
Immunoglobulin lambda joining 1	A0A0A0MT76	42	PSRLLLQPSPQRADPRCWP RGFWSEPQSLCYVFGTGTK VTVL
Keratin-associated protein 22-1	Q3MIV0	48	MSFDNNYHGGQGYAKGG LGCSYGCGLSGYGYACYC PWCYERSWFSGCF
Leydig cell tumor 10 kDa protein homolog	Q9UNZ5	99	MAQGQRKFQAHKPAKSKT AAAASEKNRGPRKGGRVI APKKARVVQQQLKKNLE VGIRKKIEHDVVMKASSSL PKKLALLKAPAKKGAAA ATSSKTPS
MIEF1 upstream open reading frame protein	L0R8F8	70	MAPWSREAVLSLYRALLR QGRQLRYTDRDFYFASIRR EFRKNQKLEDAEARERQL EKGLVFLNGKLGRII
MHC class I related sequence A	A0A0M3LCT1	23	MGLGPVFLLLAGIFPFAPP GAAA

Minor histocompatibility protein HB-1	O97980	41	MEEQPECREEKRGSLHVW KSELVEVEDDVYLRHSSSL TYRL
Myoregulin	P0DMT0	46	MTGKNWILISTTTPKSLED EIVGRLLKILFVIFVDLISIY VVITS
NLR family pyrin domain-containing protein 2B	P0DMW2	45	MVSSAQLDFNLQALLGQL SQDDLCKFKSLIRTVSLGN ELQKIPQT
Negative regulator of P-body association	A0A0U1RRE5	68	MGDQPCASGRSTLPPGNA REAKPPKKRCLLAPRWDY PEGTPNGGSTTLPAPPAS AGLKSHPPPPEK
Oculomedin	Q9Y5M6	44	MGMYPPLLKIYLSRHISIL FYLKILYKSGIIWLSWYSFI LLVL
Phorbol-12-myristate-13-acetate-induced protein 1	Q13794	54	MPGKKARKNAQPSPARAP AELEVECATQLRRFGDKL NFRQKLLNLISKLFCSGT
Cardiac phospholamban	P26678	52	MEKVQYLTRSAIRRASIE MPQQARQKLQNLFINFCLI LICLLLICIIVMLL
Photoreceptor disk component PRCD	Q00LT1	54	MCTTLFLLSTLAMLWRRR FANRVQPEPSDVGARG SSLDADPQSSGREKEPLK
Protein PIGBOS1	A0A0B4J2F0	54	MFRRLTFAQLLFATVLGIA GGVYIFQPVFEQYAKDQK ELKEKMQLVQESEEKKS
Putative uncharacterized protein PRO2829	Q9P1C3	46	MVRPHLLKKKILGRVWWL MPVVLALWEAEVGGSLEV RSLRPAWPTW
Putative DNA-binding protein inhibitor ID-2B	Q14602	36	MKAfspVRSIRKNSLLDHR LGISQSKEPVDDLMSLL

Putative glycosylation-dependent cell adhesion molecule 1	Q8IVK1	47	MKFFMVLLPASLASTSLAI LDVESGLPQLSVLLSNRL RGKTCQTGP
Putative makorin-5	Q6NVV0	33	MLLA AVG DDE LTDSEDES DLFHEELED FYDLDL
Putative tumor antigen NA88-A	P0C5K6	33	MSPPSSM CSPV PLLAASG QRMTQGQHFLQKV
Sarcolipin	O00631	31	MGINTRELFLNFTIVLITVIL MWLLVRSYQY
Short transmembrane mitochondrial protein 1	E0CX11	47	MLQFLLGFTLGNVVGMYL AQNYDIPNLAKKLEEKKD LDAKKPPSA
Small cysteine and glycine repeat-containing protein 10	A0A286YEX9	47	MGCCGC GGC GGC RCGC GGC GGG CGG CGG CGG C GCG GCG SYTTCR
Small integral membrane protein 38	A0A286YFK9	51	MTSWPGGSFGPDPLLALLV VILLARLILWSCLGTYIDYR LAQRRPQPKQD
Spermatid nuclear transition protein 1	P09430	55	MSTS RKLKSHGMRRSKR SPHKGVKRGGSKRKYRKG NLKS RKG DDANRNYRSH L
Thymosin beta-15A	P0CG34	45	MSDKPDLSEVEKFDRSKLK KTNT EKNTLPSKETIQQE KECVQTS
Mitochondrial import receptor subunit TOM5 homolog	Q8N4H	51	MFRIEGLAPKLDPEEMKRK MREDVISSIRNFLIYVALLR VTPFILKKLDI
V-alpha-13	A0N7E1	23	ASQGRKLD SYI WKRKPAL LFHPY
Putative peptide YY-2	Q9NRI6	33	MATVLL ALLV YL GALVDA YPIKPEAPGEDAFLG

We obtained the structures predicted by the three methods using their default parameters on the University of Utah Center for High Performance Computing research clusters. In all cases we considered for the comparisons presented here the best structure as reported by the methods used. Structures for 60S ribosomal, Conotoxin, Humanin, and MHC class I related sequence A were predicted only with AlphaFold and I-TASSER because they are too short to be predicted by ROSETTA.

We used STRIDE (26) to extract the secondary structure assignments of all the structures considered here. The secondary structures were classified in an 8-state secondary structure description, including  $\alpha$ -helix (H), residue in isolated  $\beta$ -bridge (B), extended strand in parallel and/or antiparallel b-sheet conformation (E), 310 helix (G), 5-helix (I), turn (T), bend (S), and coil/loops and irregular elements (C). The gyration radius of each microprotein was calculated with an R script using Bio3D (27) with each corresponding PDB file and all the comparison and structure figures were done using ChimeraX (28-30) with the default parameters.

## Results

All FASTA files and predicted structures and their comparisons are available as .cxs files at <https://zenodo.org/records/14501968>. The comparison of the predicted structures using the three approaches considered here with the three available experimental ones are given in Table 2. The comparison of the predicted structures among the three methods considered here are given in Table 3 (I-TASSER and AlphaFold), Table 4 (I-TASSER and ROSETTA) and Table 5 (AlphaFold and ROSETTA). Table 6 presents the comparison of the predicted structures by I-TASSER and AlphaFold, for those microproteins for which the ROSETTA structures could not be calculated. In all tables we present the values of RMS Pruned, # Pruned (number of AA in the

pruned sector), % Pruned (percentage of AA in the pruned sector) and RMS All (RMS including all AA in the microprotein). The pruned values correspond to the overlap of a sequence of amino acids (larger than 3) for which the overlap is the best. Their matching quality is given by RMS Pruned and the length and relative length of the pruned segment by #Pruned, and %Pruned, respectively. Finally the RMS All is the measure of the difference between the entire sequences of amino acids (28-30). All the RMS values are given in Å.

The analysis of the results in Table 2, shows an average RMS between predicted and experimental structures of 4.43 Å, 6.84 Å and 12.20 Å for the predicted structures using AlphaFold, I-TASSER and ROSETTA, respectively. This is in general agreement with recent CASP (15) results showing that AlphaFold is the most reliable method for protein structure prediction. But the average value of 4.43 Å is substantially larger than accuracies below 1 Å that have been reported for AlphaFold (12). It is difficult to make any strong conclusion of a comparison of only three structures, but the lack of microprotein structures in the AlphaFold training sets may be the root cause of this discrepancy. Clearly it is of critical importance to find a much larger set of microprotein structures to facilitate the comparison as well as retraining prediction models to better represent these systems. In other hand the results for both I-TASSER and AlphaFold for the pruned comparison show consistent sub 1 Å overlaps for pruned regions ranging from 50% to 97% of the corresponding sequences. This shows that the methods may be able to reproduce the folding of the core of the microprotein but have substantial dissimilarities at the end regions. This is apparent by examination of the pictorial comparison of structures presented in Figure 1.

Table 3 shows that comparison of the I-TASSER and AlphaFold predicted structures for the larger structures included in all the comparisons, showing good agreement, average RMS =

0.70 Å, for the pruned regions which on average are 32% of the microprotein. Similar values average RMS = 0.85 Å for the pruned region (45%) and overall average RMS = 7.8 Å are observed for the smaller microproteins (Table 6) for which ROSETTA predictions were not possible. Similar results are also observed for comparisons between I-TASSER and ROSETTA structures (Table 4), average RMS = 0.97 Å, for the pruned regions which on average are 28% of the microprotein and an overall average RMS = 11.12 Å. For the comparisons between AlphaFold and ROSETTA (Table 5), we find average RMS = 0.93 Å, for the pruned regions which on average are 26% of the microprotein and an overall average RMS = 22.60 Å. The pruned regions for which there is good overlap range from 5% to 100%.

Some examples of the structures within this range are presented in Figure 2. For Sarcolipin the percentage of pruned regions with good overlap are 100%, 65%, and 65% for the I-TASSER/AlphaFold, I-TASSER/ROSETTA and ROSETTA/AlphaFold comparisons, respectively. For B melanoma antigen 4 the percentage of pruned regions with good overlap are 51%, 26%, and 31% for the TASSER/AlphaFold, I-TASSER/ROSETTA and ROSETTA/AlphaFold comparisons, respectively. For Hemotin the percentage of pruned regions with good overlap are 32%, 22%, and 8% for the TASSER/AlphaFold, I-TASSER/ROSETTA and ROSETTA/AlphaFold comparisons, respectively. For Negative regulator of P-body association the percentage of pruned regions with good overlap are only 7%, 13%, and 9% for the TASSER/AlphaFold, I-TASSER/ROSETTA and ROSETTA/AlphaFold comparisons, respectively. All the overlaps can be found in 10.5281/zenodo.14501968, and their examination shows that, as in Figure 2 (except for Negative regulator of P-body association) there is core region with dominated by a helix structure that is reproduced reasonably well by all methods and that define the pruned region of good agreement. The end of the microprotein shows very

disorganized regions and in these regions, there is much more disagreement between the methods considered here. For the Negative regulator of P-body, in which there is not helix core there is a great deal of inconsistent results for the highly disordered regions of the entire microprotein and consequently the pruned regions of good match are very small. This is consistent with the results presented previously (24) showing that the secondary structure of the microprotein are dominated by  $\alpha$  Helix conformations.

**Table 2.** Comparison of the Predicted Structure with those Available Experimentally by NMR Measurements:

Beta-theraphotoxin-Cm1a (<https://www.rcsb.org/structure/6BR0#entity-1>); Dolichyl-diphosphooligosaccharide-protein glycosyltransferase subunit 4 (<https://www.rcsb.org/structure/2LAT#entity-1>); Sarcoplasmic/endoplasmic reticulum calcium ATPase regulator DWORF (<https://www.rcsb.org/structure/7MPA#entity-1>). RMS values in Å.

### AlphaFold

	RMS Pruned	# Pruned	% Pruned	RMS All
Beta-theraphotoxin-Cm1a	0.955	32	97%	1.103
Dolichyl-diphosphooligosaccharide-protein glycosyltransferase subunit 4	0.997	18	49%	7.023
Sarcoplasmic/endoplasmic reticulum calcium ATPase regulator DWORF	0.617	22	63%	5.17

### I-TASSER

Beta-theraphotoxin-Cm1a	0.85	27	82%	1.476
Dolichyl-diphosphooligosaccharide-protein glycosyltransferase subunit 4	0.877	20	54%	15.053
Sarcoplasmic/endoplasmic reticulum calcium ATPase regulator DWORF	0.846	23	66%	3.995

### ROSETTA

Beta-theraphotoxin-Cm1a	1.369	18	55%	4.609
Dolichyl-diphosphooligosaccharide-protein glycosyltransferase subunit 4	0.888	14	38%	17.432
Sarcoplasmic/endoplasmic reticulum calcium ATPase regulator DWORF	0.462	11	31%	16.198

**Figure 1.** Comparison of the Predicted and Experimental Structures of (from Left to Right) Beta-theraphotoxin-Cm1a, Dolichyl-diphosphooligosaccharide-protein glycosyltransferase subunit 4, and Sarcoplasmic/endoplasmic reticulum calcium ATPase regulator DWORF. Pink (Experimental), Beige (AlphaFold), Blue (I-TASSER), Green (ROSETTA).

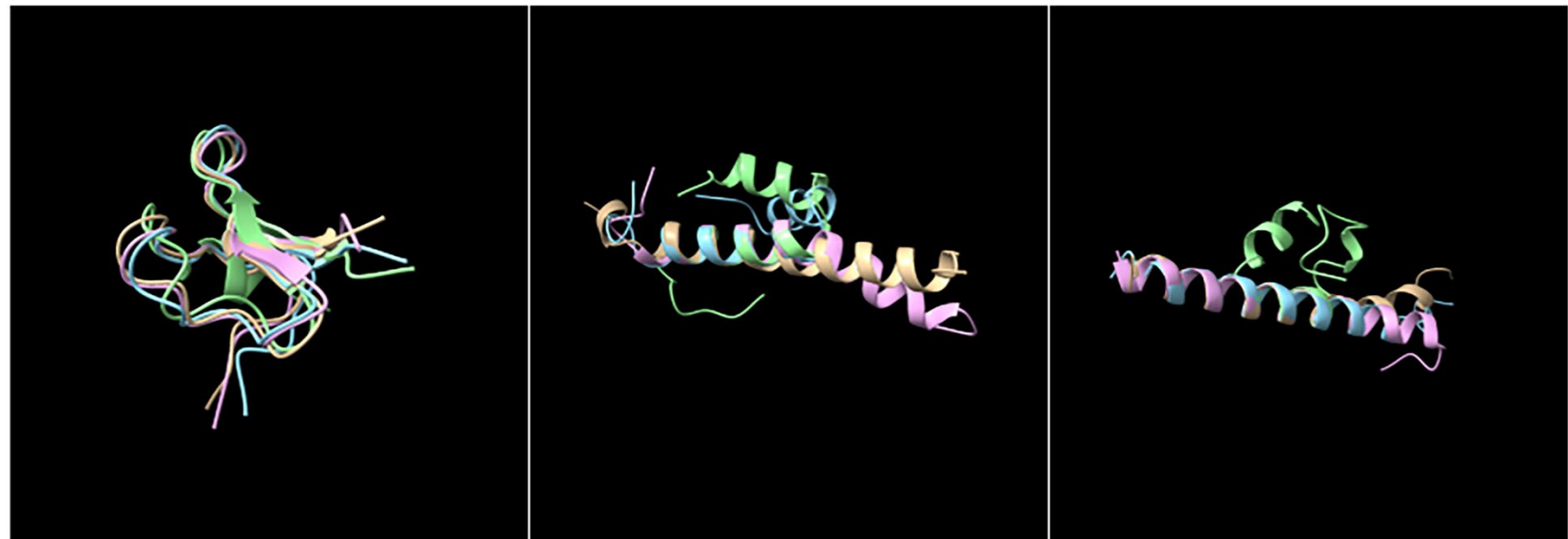


**Table 3.** Comparison of I-TASSER and AlphaFold Predicted Structures. RMS values in Å.

	RMS Pruned	# Pruned	% Pruned	RMS All
Apelin receptor early endogenous ligand	0.556	12	22%	30.626
ATP synthase subunit epsilon, mitochondrial	0.699	17	33%	16.215
B melanoma antigen 4	0.448	20	51%	25.597
Small integral membrane protein 22	0.577	20	24%	27.071
DDIT3 upstream open reading frame	0.373	22	65%	12.02
Putative protein FAM66E	1.192	12	26%	19.325
Putative gastric cancer-related gene 224 protein	0.327	27	77%	6.556
Hemotin	0.841	28	32%	29.722
Histatin-3	0.794	15	29%	41.655
Immunoglobulin lambda joining 1	0.804	9	21%	18.895
Keratin-associated protein 22-1	0.911	5	10%	36.382
Leydig cell tumor 10 kDa protein homolog	0.359	25	25%	36.75
MIEF1 upstream open reading frame protein	0.589	17	24%	8.702
Minor histocompatibility protein HB-1	1.079	6	15%	34.169
Myoregulin	0.599	25	54%	20.54
NLR family pyrin domain-containing protein 2B	0.868	22	49%	13.272
Negative regulator of P-body association	1.491	5	7%	37.757
Oculomedin	0.255	16	36%	20.903
Phorbol-12-myristate-13-acetate-induced protein 1	0.451	20	37%	27.711
Cardiac phospholamban	0.821	14	27%	21.702
Photoreceptor disk component PRCD	0.324	18	33%	29.714
Protein PIGBOS1	0.207	13	24%	26.465
Putative uncharacterized protein PRO2829	0.194	12	26%	24.011
Putative DNA-binding protein inhibitor ID-2B	1.197	7	19%	15.845

Putative glycosylation-dependent cell adhesion molecule 1	0.766	14	30%	15.08
Putative makorin-5	1.074	15	45%	7.602
Putative tumor antigen NA88-A	0.279	3	9%	30.445
Sarcolipin	0.724	31	100%	0.724
Short transmembrane mitochondrial protein 1	0.457	17	36%	17.07
Small cysteine and glycine repeat-containing protein 10	1.169	5	11%	15.948
Small integral membrane protein 38	0.789	34	67%	12.563
Spermatid nuclear transition protein 1	1.02	3	5%	17.903
Thymosin beta-15A	0.933	8	18%	27.513
Mitochondrial import receptor subunit TOM5 homolog	0.618	21	41%	21.037
Putative peptide YY-2	0.549	21	64%	16.784

**Table 4.** Comparison of I-TASSER and ROSETTA Predicted Structures. RMS values in Å.

	<b>RMS Pruned</b>	<b># Pruned</b>	<b>% Pruned</b>	<b>RMS All</b>
Apelin receptor early endogenous ligand	0.891	22	41%	6.441
ATP synthase subunit epsilon, mitochondrial	1.088	14	27%	11.063
B melanoma antigen 4	0.255	10	26%	15.381
Small integral membrane protein 22	1.475	7	8%	20.044
DDIT3 upstream open reading frame	1.073	6	18%	14.612
Putative protein FAM66E	1.118	11	23%	14.691
Putative gastric cancer-related gene 224 protein	0.639	7	20%	16.691
Hemotin	0.77	19	22%	24.722
Histatin-3	1.399	6	12%	11.018
Immunoglobulin lambda joining 1	1.568	9	21%	8.271
Keratin-associated protein 22-1	1.055	6	13%	7.132
Leydig cell tumor 10 kDa protein homolog	0.701	33	33%	13.896
MIEF1 upstream open reading frame protein	1.283	13	19%	8.239
Minor histocompatibility protein HB-1	0.908	7	17%	8.789
Myoregulin	0.959	16	35%	10.431
NLR family pyrin domain-containing protein 2B	1.001	20	44%	11.015
Negative regulator of P-body association	1.534	9	13%	11.231
Oculomedin	0.596	14	32%	14.478
Phorbol-12-myristate-13-acetate-induced protein 1	0.591	15	28%	7.141
Cardiac phospholamban	1.127	21	40%	8.233
Photoreceptor disk component PRCD	1.131	6	11%	9.801
Protein PIGBOS1	0.612	20	37%	7.858
Putative uncharacterized protein PRO2829	1.132	6	13%	10.616
Putative DNA-binding protein inhibitor ID-2B	1.11	7	19%	8.757

Putative glycosylation-dependent cell adhesion molecule 1	0.843	10	21%	10.404
Putative makorin-5	0.863	14	42%	7.24
Putative tumor antigen NA88-A	0.698	12	36%	5.841
Sarcolipin	0.533	20	65%	8.588
Short transmembrane mitochondrial protein 1	0.785	19	40%	5.023
Small cysteine and glycine repeat-containing protein 10	1.479	9	19%	9.075
Small integral membrane protein 38	0.878	29	57%	8.239
Spermatid nuclear transition protein 1	1.261	5	9%	20.577
Thymosin beta-15A	0.664	10	22%	12.182
Mitochondrial import receptor subunit TOM5 homolog	1.148	19	37%	9.002
Putative peptide YY-2	0.712	14	42%	12.413

**Table 5.** Comparison AlphaFold and ROSETTA Predicted Structures. RMS values in Å.

	RMS Pruned	# Pruned	% Pruned	RMS All
Apelin receptor early endogenous ligand	0.43	20	37%	35.338
ATP synthase subunit epsilon, mitochondrial	1.149	17	33%	14.596
B melanoma antigen 4	0.484	12	31%	27.371
Small integral membrane protein 22	0.927	27	33%	29.109
DDIT3 upstream open reading frame	1.211	4	12%	17.956
Putative protein FAM66E	1.522	6	13%	21.301
Putative gastric cancer-related gene 224 protein	0.785	8	23%	19.639
Hemotin	1.393	7	8%	28.39
Histatin-3	0.823	6	12%	34.628
Immunoglobulin lambda joining 1	1.204	4	10%	24.655
Keratin-associated protein 22-1	0.665	5	10%	34.704
Leydig cell tumor 10 kDa protein homolog	1.337	4	4%	26.45
MIEF1 upstream open reading frame protein	1.345	27	39%	4.279
Minor histocompatibility protein HB-1	0.611	5	12%	39.475
Myoregulin	0.789	17	37%	21.483
NLR family pyrin domain-containing protein 2B	0.693	17	38%	15.054
Negative regulator of P-body association	0.878	6	9%	34.096
Oculomedin	0.7	25	57%	16.263
Phorbol-12-myristate-13-acetate-induced protein 1	0.582	18	33%	30.424
Cardiac phospholamban	0.476	13	25%	21.609
Photoreceptor disk component PRCD	0.824	20	37%	25.661
Protein PIGBOS1	1.18	14	26%	19.766
Putative uncharacterized protein PRO2829	1.209	9	20%	21.486
Putative DNA-binding protein inhibitor ID-2B	1.263	6	17%	18.485

Putative glycosylation-dependent cell adhesion molecule 1	1.354	12	26%	17.23
Putative makorin-5	1.358	6	18%	11.68
Putative tumor antigen NA88-A	0.556	4	12%	30.408
Sarcolipin	0.67	20	65%	8.316
Short transmembrane mitochondrial protein 1	0.901	17	36%	16.354
Small cysteine and glycine repeat-containing protein 10	1.117	7	15%	10.437
Small integral membrane protein 38	0.941	29	57%	17.583
Spermatid nuclear transition protein 1	0.964	7	13%	26.645
Thymosin beta-15A	0.8	9	20%	25.957
Mitochondrial import receptor subunit TOM5 homolog	0.679	18	35%	22.376
Putative peptide YY-2	0.809	16	48%	21.765

**Table 6.** Comparison AlphaFold and I-TASSER Predicted Structures, for which ROSETTA Structures could not be Calculated. RMS values in Å.

	<b>RMS Pruned</b>	<b># Pruned</b>	<b>% Pruned</b>	<b>RMS All</b>
60S ribosomal protein L41	0.335	24	96%	1.337
Conotoxin PIVE	1.196	5	21%	7.263
Humanin	1.219	3	13%	14.67
MHC class I related sequence A	0.654	12	52%	8.023

**Figure 2.** Superposition of Structures within the 5% to 100% Range of the Pruned Regions with Good Overlap. From UL clockwise, Sarcolipin (100%, 65%, 65%); B melanoma antigen 4 (51%, 26%, 31%); Hemotin (32%, 22%, 8%); Negative regulator of P-body association (7%, 13%, 9%). Between parenthesis are the % of pruned regions in the comparison between I-TASSER/AlphaFold, I-TASSER/ROSETTA, and ROSETTA/AlphaFold, respectively. Beige (AlphaFold), Blue (I-TASSER), Pink (ROSETTA).

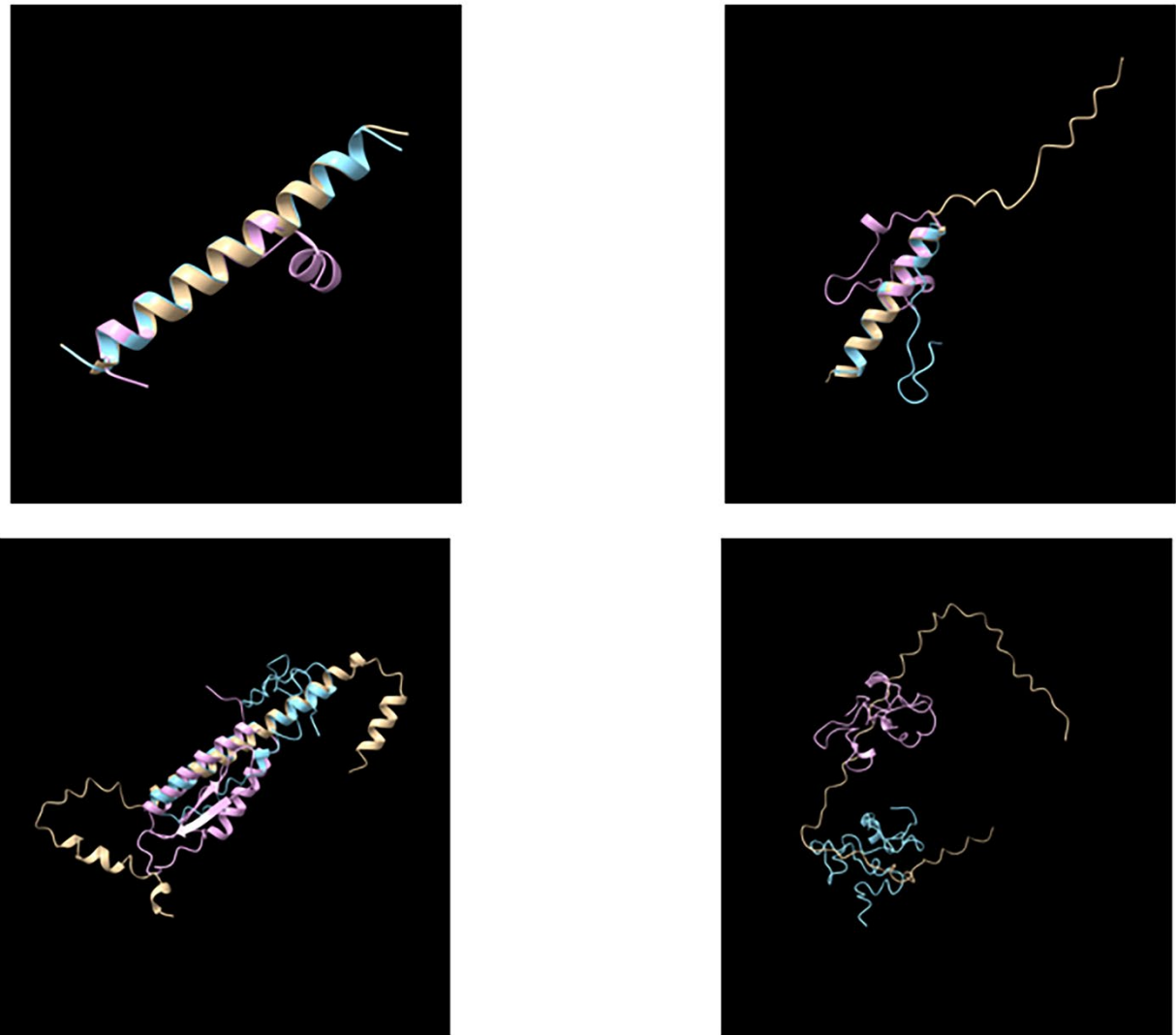
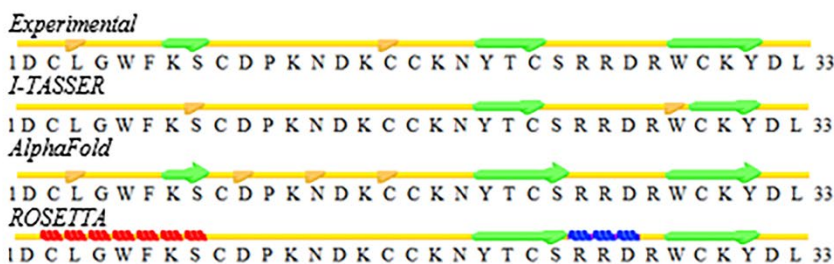


Figure 3 presents the comparison of the secondary structures predicted by the three methods considered here with the available experimental ones. The rest of the companions have been uploaded to 10.5281/zenodo.14501968. It is observed that there is a general agreement between the predicted and experimental secondary structures for the limited cases in which those are available. Except for Beta-theraphototoxin-Cm1a, the structures are dominated by  $\alpha$ -Helix folding, which is the case (see below) for most of the other microproteins studied here. Both AlphaFold and ROSETTA predict some regions with  $\beta$ -Helix folding that are not present in the experimental ones.

The inspection of the secondary structures for the microproteins studied here for which there are no experimental counterparts are given in the repository: <https://zenodo.org/records/14501968> and the following observations can be reported: there is reasonable overall agreement between the three archetypical methods used here. Overall, the structures are dominated by  $\alpha$ -Helix folding, with some minor  $\beta$ -Helix. Both the N and C terminus of the microprotein tend to exhibit turn and coil folding, which are also found linking the predominant  $\alpha$ -Helix segments. There are a few exceptions to these overall observations, DDIT3 upstream open reading frame, Putative protein FAM66E, Hemotin, Humanin, Immunoglobulin lambda joining 1, Keratin-associated protein 22-1, Minor histocompatibility protein HB-1, Negative regulator of P-body association, Small cysteine and glycine repeat-containing protein 10, for which at least one of the methods used here predicts the existence of some  $\beta$  sheets and in some cases large regions dominated by coils and turns.

**Figure 3.** Comparison of Secondary Structures for the Microproteins Studied here with Experimental Structures.

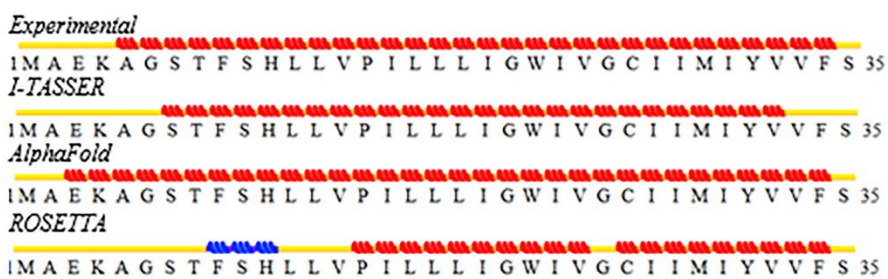
**Beta-theraphotoxin-Cmla**



**Dolichyl-diphosphooligosaccharide--protein glycosyltransferase subunit 4**



**Sarcoplasmic/endoplasmic reticulum calcium ATPase regulator DWORF**



**Legend of secondary structure icons:**

H	Alpha-Helix	T	Turn
E	Extended Configuration (Beta-sheet)	C or " " Coil	
B	Isolated Beta Bridge	G	3-10 Helix
b	Isolated Beta Bridge (Type 3 Fig 4,cd)	I	Pi-Helix

Table 7 presents the comparison of calculated and experimental ratios of gyration for all the microproteins studied here. Comparing ratios of gyration is very important because it allows us to compare the compactness of the structures predicted here. Our previous work using I-TASSER had shown that for these microprotein the radius of gyration follows a similar power law than those studied by before (31, 32), showing that the ratios of gyration of microproteins behave similarly to those of regular larger ones. Here we find that the ratios of gyration average  $19.9 \pm 6.3$  Å,  $11.4 \pm 2.4$  Å, and  $10.8 \pm 1.9$  Å, for AlphaFold, I-TASSER and ROSETTA, respectively. The values of I-TASSER show that these methods predict consistently more compact structures than AlphaFold and with an average values closer to the average for the known experimental structures of  $13.3 \pm 3.6$  Å. For the tree microproteins for which experimental structures are available, Beta-theraphotoxin-Cm1a, Dolichyl-diphosphooligosaccharide--protein glycosyltransferase subunit 4 and Sarcoplasmic/endoplasmic reticulum calcium ATPase regulator DWORF the predicted values by I-TASSER and ROSETTA are in much better agreement with the experimental values than those for AlphaFold.

**Table 7.** Comparison of Calculated and Experimental Ratios of Gyration.

	<b>I-TASSER</b>	<b>AlphaFold</b>	<b>ROSETTA</b>	<b>Experimental</b>
60S ribosomal protein L41	12.40291	11.63435	n/a	
Apelin receptor early endogenous ligand	11.32369	25.71901	11.02093	
ATP synthase subunit epsilon,mitochondrial	12.08668	16.78897	10.5146	
Beta-theraphotoxin-Cm1a	9.144739	16.44428	9.480134	9.172642
B melanoma antigen 4	11.00577	19.82223	9.041153	
Small integral membrane protein 22	12.42887	27.68764	15.20708	
Conotoxin PIVE	7.89883	10.0576	n/a	
DDIT3 upstream open reding frame	12.2987	15.28182	9.950959	
Dolichyl-diphosphooligosaccharide--protein glycosyltransferase subunit 4	10.48763	9.431157	9.810666	15.58525
Sarcoplasmic/endoplasmic reticulum calcium ATPase regulator DWORF	15.51709	15.85249	8.512639	15.06084
Putative protein FAM66E	10.49409	18.23353	9.961591	
Putative gastric cancer-related gene 224 protein	13.60397	16.57206	9.063545	
Hemotin	15.99669	28.84643	13.9568	
Histatin-3	10.95275	17.06628	10.96649	
Humanin	10.38356	11.57637	n/a	
Immunoglobulin lambda joining 1	9.810069	19.68618	9.853099	
Keratin-associated protein 22-1	9.452182	30.11635	9.687816	
Leydig cell tumor 10 kDa protein homolog	18.05543	27.2195	17.33295	
MIEF1 upstream open reading frame protein	12.10099	13.58785	12.66606	
MHC class I related sequence A	7.932696	10.30825	n/a	
Minor histocompatibility protein HB-1	11.02868	34.91297	10.5005	
Myoregulin	11.6991	20.74936	10.12426	

NLR family pyrin domain-containing protein 2B	10.23049	14.6146	9.401111
Negative regulator of P-body association	11.11929	30.27523	11.56481
Oculomedin	9.718689	19.79515	13.44144
Phorbol-12-myristate-13-acetate-induced protein 1	10.9935	26.34424	10.78076
Cardiac phospholamban	10.74269	19.87108	12.04222
Photoreceptor disk component PRCD	11.30422	22.10442	11.14949
Protein PIGBOS1	11.25238	22.88849	11.78394
Putative uncharacterized protein PRO2829	10.12429	22.31544	9.959177
Putative DNA-binding protein inhibitor ID-2B	9.361572	17.10463	9.281286
putative glycosylation-dependent cell adhesion molecule 1	9.595026	30.97979	9.706476
Putative makorin-5	9.902365	12.87667	8.904774
putative tumor antigen NA88-A	9.380111	25.18957	8.590735
Sarcolipin	14.11977	14.1449	11.45183
Short transmembrane mitochondrial protein 1	10.62308	19.0627	10.88649
Small cysteine and glycine repeat-containing protein 10	8.23885	13.29567	8.774869
small integral membrane protein 38	16.82572	23.30426	13.83696
Spermatid nuclear transition protein 1	16.75474	19.63647	12.01156
Thymosin beta-15A	10.54257	23.50567	9.783172
Mitochondrial import receptor subunit TOM5 homolog	11.00219	22.31361	10.71685
Putative peptide YY-2	9.887102	16.64908	8.991697

## Discussion and Conclusion

In this paper, we discussed the methods available for predicting the secondary and tertiary structures of microproteins and provided examples of calculations done with three archetypical methods (AlphaFold, I-TASSER and ROSETTA) predicting the structures of 44 genuine microproteins. The results show that for this set of microproteins the methods considered here show a reasonable agreement among them and with the very few cases in which experimental structures are available. None-the-less, the agreement with experimental structures is not as good as for larger proteins, indicating that is necessary to obtain a much larger set of experimental microproteins structures to better evaluate and eventually calibrate prediction methods. For the leading protein structure prediction method, AlphaFold, the average RMS value for the microproteins studied here of 4.43 Å is substantially larger than the accuracies below 1 Å that have been reported for AlphaFold (12) for larger and better characterized proteins. It is difficult to make any strong conclusion of a comparison of only three structures, but the lack of microprotein structures in the AlphaFold training sets may be the root cause of these discrepancies. Clearly it is of critical importance to find a much larger set of microprotein structures to facilitate the comparison as well as retraining prediction models to better represent these systems.

One limitation of this study is the reliance on modeling tools originally developed for larger proteins, which may introduce biases in the predictions. However, due to the limited availability of experimentally determined microprotein structures, it is currently not possible to refine these tools specifically for microproteins.

**Conflict of Interest:** The author does not have any conflict of interest to declare. Microsoft co-Pilot was used to rewrite parts of the manuscript for clarity and to avoid verbatim repletion of previously published paragraphs from Ref. 23. Finally, co-Pilot was used to assure that there was no duplicated text from the literature.

## References

1. Ma J, Ward CC, Jungreis I, Slavoff SA, Schwaid AG, Neveu J, et al. Discovery of Human sORF-Encoded Polypeptides (SEPs) in Cell Lines and Tissue. *Journal of Proteome Research*. 2014;13(3):1757-65. doi: 10.1021/pr401280w.
2. Rathore A, Martinez TF, Chu Q, Saghatelian A. Small, but mighty? Searching for human microproteins and their potential for understanding health and disease. *Expert review of proteomics*. 2018;15(12):963-5. Epub 2018/11/15. doi: 10.1080/14789450.2018.1547194. PubMed PMID: 30415582.
3. Saghatelian A, Couso JP. Discovery and characterization of smORF-encoded bioactive polypeptides. *Nature Chemical Biology*. 2015;11(12):909-16. doi: 10.1038/nchembio.1964.
4. Mohsen JJ, Martel AA, Slavoff SA. Microproteins-Discovery, structure, and function. *Proteomics*. 2023;23(23-24):e2100211. Epub 20230821. doi: 10.1002/pmic.202100211. PubMed PMID: 37603371; PubMed Central PMCID: PMC10841188.
5. Berman HM, Westbrook J, Feng Z, Gilliland G, Bhat TN, Weissig H, et al. The Protein Data Bank. *Nucleic Acids Research*. 2000;28(1):235-42. doi: 10.1093/nar/28.1.235.
6. Kryshtafovych A, Schwede T, Topf M, Fidelis K, Moult J. Critical assessment of methods of protein structure prediction (CASP)—Round XIII. *Proteins: Structure, Function, and Bioinformatics*. 2019;87(12):1011-20. doi: 10.1002/prot.25823.
7. Kryshtafovych A, Venclovas Č, Fidelis K, Moult J. Progress over the first decade of CASP experiments. *Proteins: Structure, Function, and Bioinformatics*. 2005;61(S7):225-36. doi: 10.1002/prot.20740.

8. Moult J, Fidelis K, Kryshtafovych A, Schwede T, Tramontano A. Critical assessment of methods of protein structure prediction (CASP)—round x. *Proteins: Structure, Function, and Bioinformatics*. 2014;82(S2):1-6.

9. Moult J, Fidelis K, Zemla A, Hubbard T. Critical assessment of methods of protein structure prediction (CASP): Round IV. *Proteins: Structure, Function, and Bioinformatics*. 2001;45(S5):2-7. doi: 10.1002/prot.10054.

10. Kaczanowski S, Zielenkiewicz P. Why similar protein sequences encode similar three-dimensional structures? *Theoretical Chemistry Accounts*. 2010;125(3):643-50. doi: 10.1007/s00214-009-0656-3.

11. Liang J, Naveed H, Jimenez-Morales D, Adamian L, Lin M. Computational studies of membrane proteins: Models and predictions for biological understanding. *Biochimica et Biophysica Acta (BBA) - Biomembranes*. 2012;1818(4):927-41. doi: <https://doi.org/10.1016/j.bbamem.2011.09.026>.

12. Jumper J, Evans R, Pritzel A, Green T, Figurnov M, Ronneberger O, et al. Highly accurate protein structure prediction with AlphaFold. *Nature*. 2021;596(7873):583-9. doi: 10.1038/s41586-021-03819-2.

13. Varadi M, Anyango S, Deshpande M, Nair S, Natassia C, Yordanova G, et al. AlphaFold Protein Structure Database: massively expanding the structural coverage of protein-sequence space with high-accuracy models. *Nucleic Acids Research*. 2022;50(D1):D439-D44. doi: 10.1093/nar/gkab1061.

14. Runthala A. Protein structure prediction: challenging targets for CASP10. *J Biomol Struct Dyn*. 2012;30(5):607-15. Epub 2012/06/27. doi: 10.1080/07391102.2012.687526. PubMed PMID: 22731875.

15. Kryshtafovych A, Schwede T, Topf M, Fidelis K, Moult J. Critical assessment of methods of protein structure prediction (CASP)—Round XV. *Proteins: Structure, Function, and Bioinformatics*. 2023;91(12):1539-49. doi: <https://doi.org/10.1002/prot.26617>.

16. Zhang Y. I-TASSER server for protein 3D structure prediction. *BMC Bioinformatics*. 2008;9:40. Epub 2008/01/25. doi: 10.1186/1471-2105-9-40. PubMed PMID: 18215316; PubMed Central PMCID: 2245901.

17. Roy A, Kucukural A, Zhang Y. I-TASSER: a unified platform for automated protein structure and function prediction. *Nat Protocols*. 2010;5(4):725-38.

18. Lab YZ. I-TASSER FAQ, #10. Available from: <https://zhanglab.ccmb.med.umich.edu/I-TASSER/FAQ.html#10>.

19. Yang J, Yan R, Roy A, Xu D, Poisson J, Zhang Y. The I-TASSER Suite: protein structure and function prediction. *Nature Methods*. 2015;12:7-8. doi: 10.1038/nmeth.3213.

20. Rohl CA, Strauss CE, Misura KM, Baker D. Protein structure prediction using Rosetta. *Methods in enzymology*. 383: Elsevier; 2004. p. 66-93.

21. Leaver-Fay A, Tyka M, Lewis SM, Lange OF, Thompson J, Jacak R, et al. ROSETTA3: an object-oriented software suite for the simulation and design of macromolecules. *Methods Enzymol*. 2011;487:545-74. Epub 2010/12/29. doi: 10.1016/b978-0-12-381270-4.00019-6. PubMed PMID: 21187238.

22. Das R, Qian B, Raman S, Vernon R, Thompson J, Bradley P, et al. Structure prediction for CASP7 targets using extensive all-atom refinement with Rosetta@ home. *Proteins: Structure, Function, and Bioinformatics*. 2007;69(S8):118-28.

23. Kim DE, Chivian D, Baker D. Protein structure prediction and analysis using the Robetta server. *Nucleic acids research*. 2004;32(suppl\_2):W526-W31.

24. Thambu K, Glomb V, Hernandez Trapero R, Facelli JC. Microproteins: A 3D protein structure prediction analysis. *Journal of Biomolecular Structure and Dynamics*. 2022;40(24):13738-46.

25. Wu CH, Apweiler R, Bairoch A, Natale DA, Barker WC, Boeckmann B, et al. The Universal Protein Resource (UniProt): an expanding universe of protein information. *Nucleic acids research*. 2006;34(Database issue):D187-91.

26. Heinig M, Frishman D. STRIDE: a web server for secondary structure assignment from known atomic coordinates of proteins. *Nucleic Acids Res*. 2004;32(Web Server issue):W500-2. Epub 2004/06/25. doi: 10.1093/nar/gkh429. PubMed PMID: 15215436; PubMed Central PMCID: PMC441567.

27. Grant BJ, Rodrigues APC, ElSawy KM, McCammon JA, Caves LSD. Bio3d: an R package for the comparative analysis of protein structures. *Bioinformatics*. 2006;22(21):2695-6. doi: 10.1093/bioinformatics/btl461.

28. Pettersen EF, Goddard TD, Huang CC, Meng EC, Couch GS, Croll TI, et al. UCSF ChimeraX: Structure visualization for researchers, educators, and developers. *Protein Sci*. 2021;30(1):70-82. Epub 20201022. doi: 10.1002/pro.3943. PubMed PMID: 32881101; PubMed Central PMCID: PMC7737788.

29. Pettersen EF, Goddard TD, Huang CC, Couch GS, Greenblatt DM, Meng EC, et al. UCSF Chimera—A visualization system for exploratory research and analysis. *Journal of Computational Chemistry*. 2004;25:1605-12. doi: 10.1002/jcc.20084.

30. Goddard TD, Huang CC, Meng EC, Pettersen EF, Couch GS, Morris JH, et al. UCSF ChimeraX: Meeting modern challenges in visualization and analysis. *Protein Sci*. 2018;27(1):14-

25. Epub 20170906. doi: 10.1002/pro.3235. PubMed PMID: 28710774; PubMed Central  
PMCID: PMC5734306.

31. Hong L, Lei J. Scaling law for the radius of gyration of proteins and its dependence on  
hydrophobicity. *Journal of Polymer Science Part B: Polymer Physics*. 2009;47(2):207-14. doi:  
10.1002/polb.21634.

32. Tanner JJ. Empirical power laws for the radii of gyration of protein oligomers. *Acta  
Crystallogr D Struct Biol*. 2016;72(Pt 10):1119-29. Epub 20160915. doi:  
10.1107/s2059798316013218. PubMed PMID: 27710933; PubMed Central PMCID:  
PMC5053138.